Single-Substrate Transmissive Antenna Radiating Arbitrary Symmetric Multibeams Based on Coding Metasurface

Pengfei Zhang, Xinwei Chen, and Wenmei Zhang, *Senior Member, IEEE*

***Abstract*—In this letter, an approach to designing the symmetric multibeam metasurface (MS) based on 1-bit coding sequences is put forward and its effectiveness is verified. Also, a single-substrate element with the transmissive coefficient of −0.63 dB is designed to reduce the profile and improve the gain. Moreover, the amplitude and the phase of the element could be regulated independently so that the element could be employed to suppress the sidelobe level (SLL). Finally, based on the proposed approach and the element, a low SLL transmissive dual-beam antenna employing a single-substrate coding MSs is constructed. The measured result shows that, at 15 GHz, the antenna has a gain of 15.9 dBi and SLL of −16.9 dB. The −1.5 dB gain bandwidth of the antenna is from 14.78 to 18 GHz.**

***Index Terms*—Coding metasurface (CMS), phase and amplitude modulation, single-substrate, transmissive metasurface (MS).**

I. Introduction

THE concept of digital coding metasurfaces (CMSs) was first proposed by Cui et al. [1]. CMSs can realize the digital regulation of electromagnetic waves (EMWs) by denoting the elements with phase responses of 0, $\pi/2$, π, and $3\pi/2$ as "00," "01," "10," and "11." Liu et al. [2] further enriched the theory of CMSs by introducing the convolution theorem. For example, for the conventional method, the original CMSs formed by 1-bit coding sequences can radiate the beam with $\theta = \arcsin(\lambda/\Gamma)$ (here, λ is the free-space wavelength, Γ is the periodicity of the gradient coding sequence, and θ is the elevation angle of the beam). Assuming that four coding sequences c_1, c_2, c_3, and c_4 are "0101 …," "00110011 …," "000111000 …," and "000011110000 …," respectively. Then, in the case that the periodic length of the element is 8 mm, θ generated by c_2, c_3, and c_4 are 38.68°, 24.62°, and 18.21° at 15 GHz [Since Γ of c_1 is smaller than λ, the incident wave will be converted to the surface wave propagating along the metasurface (MS)]. If the convolution theorem is added, θ will be "70°, 60°, 56.39°, 53.46°, 46.76°, 41.68°, 38.6°, 36.47°, 34.15°, 31.35°, and 29° …." It is indicated that, although the convolution theorem does enrich the achievable θ, θ is still discrete. Arbitrary and continuous θ cannot be achieved using 1-bit coding sequences. Also, with the increase of θ, gaps between the adjacent θ get larger and larger.

In addition, for a transmissive MS, a multilayer structure, such as a "metal-substrate–metal-substrate–metal …" structure, was often used to obtain a high transmissive coefficient [3], [4], [5], which would undoubtedly increase cost and complexity. In recent years, some single-layer transmissive MSs have been presented [6], [7]. However, transmissive coefficients need to be further improved.

In this letter, a type of transmissive multibeam CMS antenna radiating arbitrary symmetric beams is proposed. First, an approach using 1-bit CMSs to realize symmetric multibeam is presented. Then, a split C-shaped element with a high transmissive coefficient (−0.63 dB) is designed. Next, numerical calculations and full-wave simulations are adopted to verify the effectiveness of the proposed method, respectively. Finally, a low SLL transmissive antenna based on CMSs is simulated, fabricated, and measured. The measured results show that the realized antenna can radiate the beam pointing to ±34° with a gain of 15.9 dBi and SLL of −16.9 dB at 15 GHz. The −1.5 dB gain bandwidth of the antenna is from 14.78 to 18 GHz.

II. Design Method and Verification

In this section, a method of designing CMS radiating arbitrary symmetric multibeams using a 1-bit coding sequence is proposed. Then, to verify the proposed method, a single-substrate element with high transmissive coefficients is designed. Finally, the feasibility of the method is verified through numerical calculations and full-wave simulations.

A. Design Method

Considering that the symmetric beams whose azimuth angle (φ) differs by π, the (θ, φ) of the N beams can be set to be $\{(\theta_1, \varphi_1), (\theta_1, \varphi_1+\pi), \ldots, (\theta_n, \varphi_n), (\theta_n, \varphi_n+\pi)\}$ ($N = 2n$). The phase ϕ_i for the ith beam ($1 \le i \le N$) is [8]

$$\phi_i = \varphi_0 - \frac{2\pi}{\lambda}(x \times p \times \sin\theta_i \cos\varphi_i + y \times p \times \sin\theta_i \sin\varphi_i) \tag{1}$$

where φ_0 is one of the 1-bit phase of the element. x and y represent the (xth, yth) element. p is the periodic length of the element. Here, "$(2\pi \times p \times \sin\theta_i)/\lambda$" is denoted as "$\Delta\xi_i$." Then, based on the superposition principle [9], the final phase of the (xth, yth) element for N beams can be calculated by

$$\phi_{xy} = \text{Arg}\left\{\left(e^{j\phi_1} + e^{j\phi_2} + \cdots + e^{j\phi_N}\right)\right\}$$

Manuscript received 1 November 2023; revised 25 November 2023; accepted 27 November 2023. Date of publication 29 November 2023; date of current version 5 February 2024. This work was supported in part by the National Nature Science Foundation of China under Grant 62071282; and in part by the National Science Foundation of Shanxi Province under Grant 202203021211295. *(Corresponding author: Wenmei Zhang.)*

The authors are with the School of Physics and Electronic Engineering, Shanxi University, Taiyuan 030006, China (e-mail: 1595040095@qq.com; chenxw@sxu.edu.cn; zhangwm@sxu.edu.cn).

Digital Object Identifier 10.1109/LAWP.2023.3337499

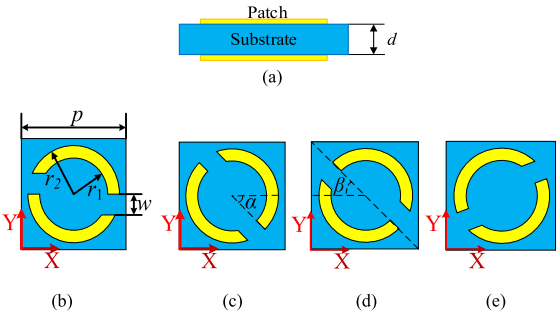

Fig. 1. Structure of the element. (a) Side view. (b) and (c) Top and bottom layers of the nonmirror element. (d) and (e) Top and bottom layers of the mirror element.

$$= \mathrm{Arg}\left\{\begin{array}{l} e^{j(\varphi_0-\Delta\xi_1\times(x\times\cos\varphi_1+y\times\sin\varphi_1))} \\ +e^{j(\varphi_0+\Delta\xi_1\times(x\times\cos\varphi_1+y\times\sin\varphi_1))} \\ +\cdots+e^{j(\varphi_0-\Delta\xi_n\times(x\times\cos\varphi_n+y\times\sin\varphi_n))} \\ +e^{j(\varphi_0+\Delta\xi_n\times(x\times\cos\varphi_n+y\times\sin\varphi_n))} \end{array}\right\}$$

$$= \mathrm{Arg}\left\{\begin{array}{l} \{2\cos\left[\Delta\xi_1\times(x\times\cos\varphi_1+y\times\sin\varphi_1)\right] \\ +\cdots+2\cos\left[\Delta\xi_n\times(x\times\cos\varphi_n+y\times\sin\varphi_n)\right]\} \\ \times e^{j\varphi_0} \end{array}\right\}$$

$$= \mathrm{Arg}\{\mathrm{Amp}_{xy}\times e^{j\varphi_0}\} \tag{2}$$

where

$$\mathrm{Amp}_{xy} = 2\cos\left[\Delta\xi_1\times(x\times\cos\varphi_1+y\times\sin\varphi_1)\right] + \cdots + 2\cos\left[\Delta\xi_n\times(x\times\cos\varphi_n+y\times\sin\varphi_n)\right]. \tag{3}$$

From (2) and (3), it can be found that the value of ϕ_{xy} will be "φ_0" or "$\varphi_0+\pi$" when "Amp$_{xy}$" is positive or negative, respectively. That is, there are only two desirable values for all ϕ_{xy}. Therefore, symmetric multibeams can be realized using the 1-bit CMSs. For example, if the Amp$_{xy}$ is positive, the phase of the (xth, yth) element is encoded as "0." Otherwise, the phase of the element is encoded as "1."

It is worth noting that the larger the size of MS is, the higher θ would be and the maximum deflecting angle θ_m can be [10]

$$\theta_m = \arcsin\left[1-0.4429\times\frac{\lambda}{N_u\times p}\right] \tag{4}$$

where N_u is the number of elements along the horizontal or orthogonal axis.

B. Element Design

In the validation phase, an element with a high transmission coefficient is designed and shown in Fig. 1. The blue part is F_4BM265 substrate ($\varepsilon_r = 2.65$ and $\tan\delta = 0.0015$), and the yellow part is the metallic pattern. The metallic pattern in the bottom layer is obtained by rotating clockwise the top one by α. w is the gap between two C-shaped elements and β is the clockwise rotation angle with respect to the x-axis. Then, 2-bit phase coverage can be achieved by adjusting w and α and the amplitude can be regulated by changing β. Other parameters are $d = 2$ mm, $p = 8$ mm, $r_1 = 2.6$ mm, and $r_2 = 3.5$ mm.

Fig. 2 shows the transmission amplitude and phase responses of the elements and the results at 15 GHz are listed in Table I. Here, the incident waves are y-polarized waves. From Fig. 2(a),

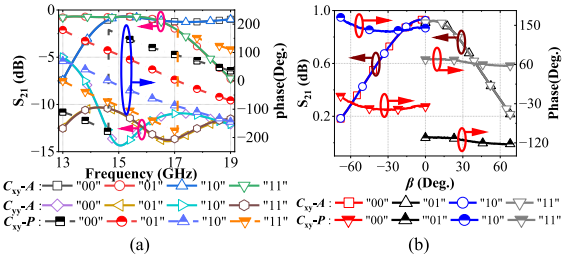

Fig. 2. Transmissive amplitude and phase with (a) frequency and (b) β.

TABLE I
PARAMETERS AND PERFORMANCE OF THE ELEMENT

Coding State	α	β	w	Mirror/ Non-mirror	Amplitude	Phase
"00"	52°	-4.5°	2.3 mm	non-mirror	0.9301	-30° (330°)
"01"	66°	4.5°	0.6 mm	non-mirror	0.928	-120°(240°)
"10"	52°	-4.5°	2.3 mm	mirror	0.930	150°
"11"	66°	4.5°	0.6 mm	mirror	0.929	60°

TABLE II
COMPARISON WITH OTHER TRANSMISSIVE AMPLITUDE/PHASE-REGULATED ELEMENTS

Ref.	Year	Substrate Layers	Polarization	Max-Amp.	Phase-Coverage
[3]	2020	3	co-pol.	0.93-1	315°
[4]	2022	2	cross-pol.	0.95-1	360°
[5]	2023	2	cross-pol.	0.85-1	360°
[6]	2022	1	cross-pol.	0.7	3 bit
[7]	2022	1	cross-pol.	0.78	360°
This work	2023	1	cross-pol.	0.93	2 bit

the cross-polarized phases (C_{xy}-P) of four elements at 15 GHz are −30° (330°), −120° (240°), 150°, and 60°, respectively, which can be used for 2-bit phase regulation. From 14.5 to 16.91 GHz, the cross-polarized amplitudes (C_{xy}-A) fluctuate near the maximum value of 0.93 (fluctuation is less than 0.1) and the copolarized amplitudes (C_{yy}-A) are less than −10 dB. The reasons for high C_{xy}-A and less fluctuation are as follows. First, the y-polarized incident waves experience multiple reflections between the top and bottom patches, such as in a Fabry–Perot resonant cavity [11], resulting in an efficient polarization conversion. Second, the proposed split C-shaped element can increase current path and enhance the coupling effect between the top and bottom patches. In Fig. 2(b), the C_{xy}-A of elements can be regulated linearly from 0.2 to 0.93 while the variation of the phase is less than 20°. Therefore, we can conclude that the split C-shaped element can be employed to independently regulate the amplitude and the phase of EMWs.

Furthermore, we compared this proposed element with other transmission-type elements with similar properties. The results are listed in Table II. It can be found that the conventional single-substrate MSs have low transmissive amplitude, while high transmissive amplitudes are achieved by stacking multilayer substrates. The proposed split C-shaped element realizes high transmissive amplitude in a single-layer substrate.

C. Verification by Numerical Calculation and Full-Wave Simulation

Symmetrical dual-beam MS arranged in 81×81 patterns is designed to verify the effectiveness of this method. The θ is

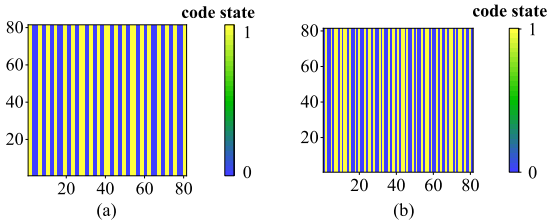

Fig. 3. 1-bit coding patterns of dual beams while (a) $\theta = \pm 35°$ and (b) $\theta = \pm 75°$.

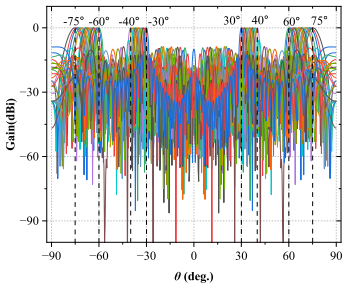

Fig. 4. Normalized radiation pattern while θ varies from $\pm 30°$ to $\pm 40°$ and from $\pm 60°$ to $\pm 75°$ at an interval of 1°.

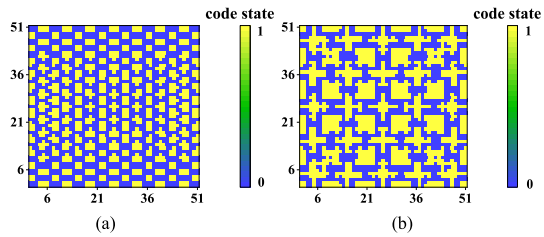

Fig. 5. 1-bit coding patterns for (a) six beams: $\{B_1: (\theta, \varphi) = (45°, 0°), B_2: (45°, 60°), B_3: (45°, 120°), B_4: (45°, 180°), B_5: (45°, 240°)$, and $B_6: (45°, 300°)\}$, and (b) eight beams: $\{B_1: (45°, 0°), B_2: (45°, 90°), B_3: (45°, 180°), B_4: (45°, 270°), B_5: (20°, 45°), B_6: (20°, 135°), B_7: (20°, 225°)$, and $B_8: (20°, 315°)\}$.

designed to vary from $\pm 30°$ to $\pm 40°$ and from $\pm 60°$ to $\pm 75°$ at an interval of 1°, while $\varphi = 0°$ or 180°. First, the 1-bit coding pattern can be obtained according to (3). Fig. 3 shows the results, while $\theta = \pm 35°$ and $\pm 75°$. Then, the normalized radiation pattern $f(\theta, \varphi)$ can be calculated as [12] follows:

$$f(\theta,\varphi) = \sum_{x=1}^{X}\sum_{y=1}^{Y} \exp\left\{-i\left\{\varphi(x,y) + \frac{2\pi}{\lambda} \times p \times \sin\theta \begin{bmatrix}(x-1/2)\cos\varphi \\ +(y-1/2)\sin\varphi\end{bmatrix}\right\}\right\} \quad (5)$$

where X and Y are the number of elements in the x- and y-directions. The other parameters are the same as those in (1). Fig. 4 shows the calculated results using MATLAB. It can be found that θ can exceed the maximum value calculated by the convolution theorem (70°) for 1-bit coding sequences and arbitrary angles less than θ_m can be realized.

Furthermore, this method can be used to design CMSs with other symmetrical multibeams, such as quad, six, or eight beams, and so on. Considering the limited space, only the results for six and eight beams are shown. Figs. 5 and 6 display the 1-bit coding patterns with 51 × 51 elements and radiation patterns simulated using CST MWS. It is indicated that the simulated

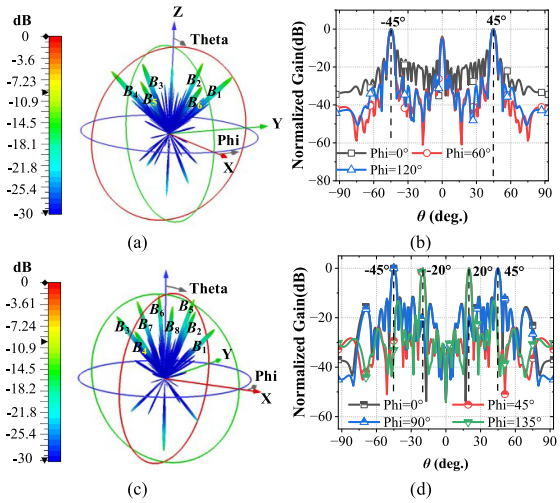

Fig. 6. Simulated radiation pattern. (a) and (c) are the 3-D results of six and eight beams, and (b) and (d) are the 2-D results of six and eight beams.

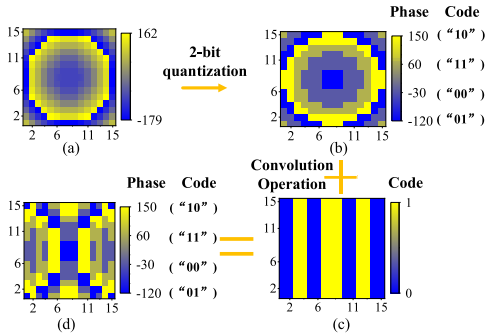

Fig. 7. Process of phase regulation. (a) Distribution of φ_{xy}. (b) 2-bit quantized pattern. (c) 1-bit pattern for the dual beams under the illumination of plane waves. (d) Final coding pattern under the illumination of the feeder.

results are in line with expectations, verifying the effectiveness of the proposed method.

III. Dual-Beam Antenna Based on a Single-Substrate CMS With Phase/Amplitude Modulation

In this section, a low SLL transmissive dual-beam antenna pointing to {(35°, 0°) and (35°, 180°)} with dimensions of 120 mm×120 mm ($6\lambda_0 \times 6\lambda_0$) is designed. A standard horn antenna *LB-62-10-C-SF* from *A-INFO* is used as the feeder and placed 90 mm below the aperture ($F/D = 0.75$). Considering that the MS is excited by plane waves in the proposed method, the spherical waves radiated by the horn antenna will be transformed into plane waves.

The detailed process of phase regulation is displayed in Fig. 7. Fig. 7(a) shows the continuous compensated phase φ_{xy} for converting spherical waves radiated by the feeder into plane waves. Here, φ_{xy} is obtained by negating the phase of the radiated wave at the position of the MS [8]. Then, φ_{xy} is further quantified into 2-bit phase (ϕ_{xy}), as shown in Fig. 7(b). (2-bit phase regulation can obtain better compensation effect than 1-bit case). The quantizing and encoding rules for ϕ_{xy} can be

TABLE III
DISTRIBUTION OF A_1

Element Number	1/15	2/14	3/13	4/12	5/11	6/10	7/9	8
A_1	0.43	0.07	0.64	0.59	0.59	0.77	0.13	1

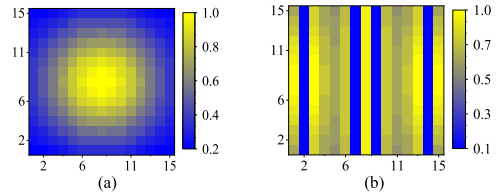

Fig. 8. Distribution of (a) I and (b) T_x.

expressed as follows:

$$\phi_{xy} = \begin{cases} -30^\circ(\text{state“00”}), & -75^\circ < \varphi_{xy} \le 15^\circ \\ -120^\circ(\text{state“01”}), & -165^\circ < \varphi_{xy} \le -75^\circ \\ 150^\circ(\text{state“10”}), & \begin{cases} -180^\circ < \varphi_{xy} \le -165^\circ, \\ 105^\circ < \varphi_{xy} \le 180^\circ \end{cases} \\ 60^\circ(\text{state“11”}), & 15^\circ < \varphi_{xy} \le 105^\circ. \end{cases} \tag{6}$$

After calculation, the average error of phase approximation is 22.5°, which is much less than 360°. Thus, the error of phase approximation has little effect on the CMSs [13]. Next, the 1-bit coding pattern for dual beams is calculated using (3) and shown in Fig. 7(c). Finally, after convolution operation [2], a 2-bit coding pattern for dual beams under the illumination of the horn antenna can be obtained, as shown in Fig. 7(d).

To suppress the SLL of the antenna, the Schelkunoff polynomial method is used to calculate excitation coefficients [8], [14]. For an N-element linear array antenna, the array factor $S(w)$ can be expressed as follows:

$$S(w) = \prod_{n=1}^{N-1} |(w - w_n)| \tag{7}$$

where w_n is the position of the roots on the unit circle. After optimizing according to the method in [8], the distribution of roots can be obtained. Here, SLL in the *xoz*-plane is set to be −20 dB and the corresponding roots are located at ±5°, ±25°, ±50°, ±105°, ±127°, ±147°, and ±160°. Then, the normalized Schelkunoff amplitudes A_1 are listed in Table III. Next, the amplitude of the (xth, yth) element $T_x(x, y)$ can be obtained by [8]

$$T_x(x,y) = \{\, [A_2(x,1) \times A_1(1,y)] \,/\, [I(x,y)/I(x,8)] \,\} \quad (1 \le x, y \le 15) \tag{8}$$

where I and T_x are both 15 × 15 matrices, as shown in Fig. 8. "$I(x,y)/I(x,8)$" is the normalized amplitude distribution of the feeder on the aperture. "A_2" is a 15 × 1 column vector of all 1, which is used to transform Schelkunoff amplitude from a 15 × 1 matrix into a 15 × 15 matrix.

Once the phase and amplitude distribution in the aperture are determined, they can be further converted into the dimensional information of the element according to Table I and Fig. 2. Then, a transmission-type dual-beam MS antenna can be constructed and denoted as MSx_{35}. Fig. 9 shows the simulated results of MSx_{35}. The results show that θ of the beams is ±34°, which is consistent with the expectation. At 15 GHz, MSx_{35} has a gain of 16.3 dBi and SLLs of −17.52 and −14.2 dB in the *xoz*- and *yoz*- planes. It is worth noting that the SLL of MSx_{35} in the *xoz*-plane is 2.48 dB higher than −20 dB, which is mainly due to the mutual coupling between the elements.

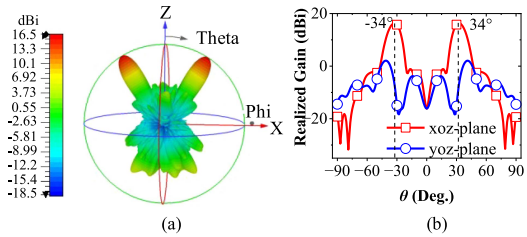

Fig. 9. Simulated results of MSx_{35}. (a) Three-dimensional result. (b) Two-dimensional result.

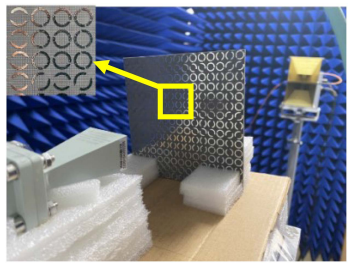

Fig. 10. Photograph of the prototype and measurement.

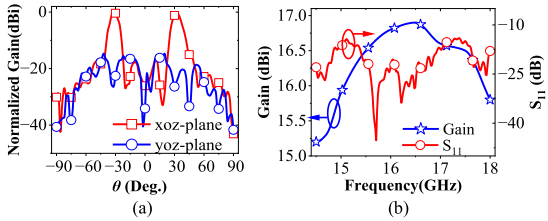

Fig. 11. Measured results of MSx_{35}. (a) Normalized gain in the *xoz*- and *yoz*-plane. (b) Gain and S_{11} with frequency.

To experimentally validate the performance of the MS$_{35}$ antenna, a prototype is fabricated and measured, as shown in Fig. 10, and the results are shown in Fig. 11. Fig. 11(a) shows the measured radiation pattern of MSx_{35} in the *xoz*- and *yoz*-plane, which is basically consistent with the simulated ones in Fig. 9. SLLs at 15 GHz are −16.9 and −13.6 dB in the *xoz*- and *yoz*-plane. Fig. 11(b) shows the gains and S_{11} of the MSx_{35}. It can be found that S_{11} of MSx_{35} is always lower than −10 dB from 14.5 to 18 GHz. At 15 GHz, MSx_{35} has a gain of 15.9 dBi. Also, the −1.5 dB gain bandwidth of the antenna is from 14.78 to 18 GHz.

IV. CONCLUSION

In this letter, an approach to designing low SLL antenna radiating arbitrary symmetric multiple beams is realized. If the element of MS has electrically adjustable phase responses, the programmable antenna with continuous scanning symmetric beams can be obtained. Furthermore, the proposed approach can also be applied to point-to-multipoint wireless communication system, providing a feasible idea in lots of multiiple-input–multiple-input (MIMO) scenarios.

REFERENCES

[1] T. J. Cui, M. Q. Qi, X. Wan, J. Zhao, and Q. Cheng, "Coding metamaterials, digital metamaterials and programmable metamaterials," *Light, Sci. Appl.*, vol. 3, Oct. 2014, Art. no. e218.

[2] S. Liu et al., "Convolution operations on coding metasurface to reach flexible and continuous controls of terahertz," *Adv. Sci.*, vol. 3, no. 10, Oct. 2016, Art. no. 1600156.

[3] R. Y. Wu et al., "Independent control of copolarized amplitude and phase responses via anisotropic metasurfaces," *Adv. Opt. Mater.*, vol. 8, no. 11, Jun. 2020, Art. no. 1902126.

[4] H. G. Hao, S. Zheng, Y. H. Tang, and X. H. Ran, "Broadband transmissive amplitude-and-phase metasurface for vortex beam generation and hologram," *Phys. Lett. A*, vol. 434, May 2022, Art. no. 128036.

[5] X. Liu, Z. Yan, E. Wang, X. Zhao, T. Zhang, and F. Fan, "Multibeam forming with arbitrary radiation power ratios based on a conformal amplitude–phase-controlled metasurface," *IEEE Trans. Antennas Propag.*, vol. 71, no. 4, pp. 3707–3712, Apr. 2023.

[6] C. L. Zheng et al., "All-dielectric trifunctional metasurface capable of independent amplitude and phase modulation," *Laser Photon. Rev.*, vol. 16, no. 7, Jul. 2022, Art. no. 2200051.

[7] Q. Li et al., "Compact anisotropic metasurface for full range and arbitrary complex-amplitude control," *IEEE Photon. J.*, vol. 14, no. 1, Feb. 2022, Art. no. 4607406.

[8] P. Zhang, W. Zhang, X. Chen, G. Han, J. Su, and R. Yang, "Low-sidelobe dual-beam antenna based on metasurface with independently regulated amplitude/phase," *IEEE Antennas Wireless Propag. Lett.*, vol. 22, no. 10, pp. 2382–2386, Oct. 2023.

[9] P. Nayeri, F. Yang, and A. Z. Elsherbeni, "Design and experiment of a single-feed quad-beam reflectarray antenna," *IEEE Trans. Antennas Propag.*, vol. 60, no. 2, pp. 1166–1171, Feb. 2012.

[10] R. C. Hansen, *Phased Array Antennas*. Hoboken, NJ, USA: Wiley, 2009, pp. 9–11.

[11] N. K. Grady et al., "Terahertz metamaterials for linear polarization conversion and anomalous refraction," *Science*, vol. 340, no. 6138, pp. 1304–1307, Jun. 2013.

[12] L.-X. Wu et al., "Transmissive metasurface with independent amplitude/phase control and its application to low-side-lobe metalens antenna," *IEEE Trans. Antennas Propag.*, vol. 70, no. 8, pp. 6526–6536, Aug. 2022.

[13] R. Y. Wu, L. Bao, L. W. Wu, and T. J. Cui, "Broadband transmission-type 1-bit coding metasurface for electromagnetic beam forming and scanning," *Sci. China Phys., Mech. Astron.*, vol. 63, no. 8, Jan. 2020, Art. no. 284211.

[14] C. A. Balanis, *Antenna Theory: Analysis and Design*. Hoboken, NJ, USA: Wiley, 2016, pp. 387–392.